Applied Catalysis B: Environmental 219 (2017) 155–162

Contents lists available at ScienceDirect

Applied Catalysis B: Environmental

journal homepage: www.elsevier.com/locate/apcatb

Palladium-exchanged small-pore zeolites with different cage systems as methane combustion catalysts

Jong Bin Lim, Donghui Jo, Suk Bong Hong*

Center for Ordered Nanoporous Materials Synthesis, Division of Environmental Science and Engineering, POSTECH, Pohang 37673, Republic of Korea

ARTICLE INFO

Article history:
Received 16 May 2017
Received in revised form 22 June 2017
Accepted 11 July 2017
Available online 15 July 2017

Keywords:
CH_4 combustion
Pd-SSZ-13
Wet conditions
Zeolite structure
Zeolite acidity

ABSTRACT

The catalytic properties of four palladium-exchanged small-pore zeolites with different cage systems (i.e., Pd-SSZ-13, Pd-LTA, Pd-PST-7, and Pd-RTH) have been evaluated for methane (CH_4) combustion and compared with those obtained from Pd-ZSM-5 and Pd-Al_2O_3 in an attempt to investigate the effects of zeolite support structure and acidity on the oxidation activity of supported Pd catalysts for this greenhouse gas. When Pd loading level was fixed to be ca. 1.0 wt%, Pd-SSZ-13 was found to show the best CH_4 oxidation activity and durability under wet feed conditions among the catalysts studied. The overall characterization results of this work demonstrate that the strong acid strength of SSZ-13 may render strong interactions between the intrazeolitic PdO species and the zeolite framework so as to effectively suppress not only PdO sintering but also dealumination during CH_4 combustion.

1. Introduction

Methane (CH_4) with a kinetic diameter of 3.8 Å, the main component of natural gas, is a cost effective and environmentally friendly fuel for natural gas vehicles (NGVs) [1]. However, the emission control of unburned CH_4 from NGV engines has been a subject of inquiry owing to its global warming potential of about 20 times in comparison with CO_2 [2]. Unfortunately, none of the catalytic systems developed thus far for complete CH_4 oxidation are efficient enough to meet the required activity standard with relatively low exhaust gas temperatures (<773 K) and a large amount of water vapor (~10 vol%) formed during engine combustion [3].

While palladium (Pd) is the most active metal for CH_4 combustion, its activity can differ notably according to the type of the support used [4]. Alumina (Al_2O_3) is one of the most widely studied metal oxides as a Pd support. When water vapor exists in the feed gas stream, however, the Pd-Al_2O_3 catalyst is severely deactivated, due to the competitive adsorption of H_2O that also results in the formation of less active $Pd(OH)_2$ [5]. In the presence of 3% water vapor, for example, its light-off temperature (T_{50}) was reported to increase from ca. 640–710 K, together with a significant decrease in CH_4 conversion after some time on stream [6]. This led to interest in the use of silica (SiO_2), hydrophobic in nature, as a support [7]. But the intrinsic CH_4 oxidation activity of Pd-SiO_2 is much lower than that of Pd-Al_2O_3 [8]. Hence, aluminosilicate zeolites, a unique class of microporous, crystalline solids, have been considered to be one possible choice for alleviating water effect on the CH_4 oxidation while achieving high catalytic activity [9].

To date, there are numerous papers on the CH_4 oxidation over zeolite-supported Pd catalysts [8–13]. However, most of them have focused on the use of medium- and large-pore zeolites like ZSM-5 (framework type MFI) and zeolite beta (*BEA) as supports. To our knowledge, in particular, few systematic studies of the water effect on the activities of zeolite-supported Pd catalysts have been reported [9]. SSZ-13 and SAPO-34 are the aluminosilicate and silicoaluminophosphate (SAPO) versions of cage-based small-pore molecular sieves with the CHA topology [14] which have been successfully commercialized as a catalyst support for the selective catalytic reduction (SCR) of NO_x with NH_3 and as a catalyst itself for the methanol-to-olefins reaction, respectively [15,16]. On the other hand, we have recently been able to synthesize the high-silica version of other cage-based small-pore zeolites such as LTA, PST-7 (UFI), and RTH using imidazolium-based organic structure-directing agents (OSDAs) [17,18]. More recently, we have demonstrated that fully copper-exchanged (Cu/Al ~ 0.50) high-silica (Si/Al = 16–23) LTA zeolites have excellent activity for NH_3-SCR even after hydrothermal aging at 1173 K, in which the current commercial Cu-SSZ-13 catalyst cannot survive [19].

Such unprecedented hydrothermal stability of Cu-LTA catalysts, as well as the commercial success of CHA-type materials, has stimulated us to use high-silica, small-pore zeolites with different cage systems as Pd supports for CH_4 oxidation. Here we evaluate

* Corresponding author.
E-mail address: sbhong@postech.ac.kr (S.B. Hong).

http://dx.doi.org/10.1016/j.apcatb.2017.07.032
0926-3373/

Table 1
Crystallographic dimensions of 8-ring windows and cages in zeolites with different pore topologies studied here.

Zeolite	IZA code	Pore dimensionality	8-ring pore size (Å) and area[a] (Å^2)	Type of cages containing 8-ring windows[b]	Cage dimensions[c] (Å) and volume[d] (Å^3)
SSZ-13	CHA	3	3.8 × 3.8, 11.3	20-hedral ([$4^{12}6^2 8^6$]) *cha* cage	8.4 × 8.4 × 8.2, 300
LTA	LTA	3	4.1 × 4.1, 13.2	26-hedral ([$4^{12}6^8 8^6$]) *lta* cage	11.4 × 11.4 × 11.4, 780
PST-7	UFI	2	4.4 × 3.6, 12.4; 3.3 × 3.3, 8.5	26-hedral ([$4^{12}6^8 8^6$]) *lta* cage	11.4 × 11.4 × 11.4, 780
RTH	RTH	2	4.1 × 3.8, 12.2; 5.6 × 2.5, 11.0	22-hedral ([$4^6 5^8 6^4 8^4$]) *t-rth* cage	10.4 × 11.1 × 9.0, 540
ZSM-5	MFI	3	(5.1 × 5.5, 22.0; 5.3 × 5.6, 23.3)	–	8.6[e]

[a] Calculated using the equation $A = \pi ab/4$, where A, a, and b are the pore area and the shortest and longest 8-ring pore diameters, respectively. The eight-ring pores in each material are assumed to be ideally circular or elliptical in shape. The values in parentheses are the 10-ring pore size and area data.
[b] In the notation [m^n...], polyhedra are defined by the n number of faces with m T-O-T edges.
[c] Obtained from the Database of Zeolite Structures [14].
[d] Calculated using the equation $V = \pi abc/6$, where V, a, b, and c are the cage size and the width, length and height of the cage, respectively. All the cages are assumed to be ideally ellipsoidal in shape.
[e] The diameter of 10-ring channel intersections.

the catalytic properties of Pd-SSZ-13, Pd-LTA, Pd-PST-7, and Pd-RTH for CH_4 combustion and compare the obtained results with those of Pd-ZSM-5 and Pd-Al_2O_3 with similar Pd contents in an attempt to understand the physicochemical requirements of zeolite supports leading to excellent catalytic performance, especially under wet feed conditions. The crystallographic dimensions of 8-ring windows and cages in these four small-pore zeolites obtained from the Database of Zeolite Structures [14], together with their cage volumes, are listed in Table 1. The physicochemical properties of supported Pd catalysts employed in this work has been characterized by powder X-ray diffraction, transmission electron microscopy, N_2 adsorption, temperature-programmed desorption of NH_3 and H_2O, ^{27}Al MAS NMR, Pd K-edge X-ray absorption near edge structure spectroscopy, and CO chemisorption.

2. Experimental

2.1. Catalyst preparation

NH_4-ZSM-5 (Si/Al = 14) and γ-Al_2O_3 with BET surface area of 200 m^2 g^{-1} were obtained from Tosoh and Sasol, respectively. Three SSZ-13 zeolites with Si/Al = 6, 16, and 27 were synthesized using N,N,N-trimethyl-1-adamantammonium as an organic structure-directing agent (OSDA) according to the procedures given elsewhere [20]. High-silica LTA (Si/Al = 16) and PST-7 (Si/Al = 11) were synthesized using 1,2-dimethyl-3-(4-methylbenzyl)imidazolium and 1,2-dimethyl-3-(2-fluorobenzyl)imidazolium in the presence of tetramethylammonium and fluoride ions, respectively, following the procedures reported in the literature [17]. RTH (Si/Al = 10) was synthesized using 1,2,3-trimethylimidazolium as an OSDA in hydroxide media [18].

As-made zeolites were calcined in air at 823 K for 8 h to remove the OSDA molecules occluded. The calcined zeolites were then converted into the ammonium form by refluxing three times in 1.0 M NH_4NO_3 solutions (1.0 g solid per 100 mL solution) for 6 h. Pd^{2+} ion-exchanged zeolites were prepared by stirring their ammonium form in 0.005 M $Pd(NO_3)_2$ solutions at 353 K for 24 h, and the Pd loading level was controlled by adjusting the amount of $Pd(NO_3)_2$ solution. Pd-Al_2O_3 was prepared by impregnating a given amount of $Pd(NO_3)_2$ onto γ-Al_2O_3. All Pd^{2+}-exchanged zeolites, as well as Pd-Al_2O_3, were dried at 373 K for 12 h and subsequently calcined in air at 773 K for 5 h. The first number of the catalyst identification indicates the Pd loading level in wt%, whereas the last number in parentheses corresponds to the bulk Si/Al ratio of the zeolite support used.

2.2. Catalysis

The steady-state CH_4 oxidation activity at 423–773 K was measured using a packed-bed flow reactor system [21], while maintaining each measurement temperature for 1 h. Two thermocouples were placed in a 1/4″ quartz tube reactor to measure the inlet and outlet gas temperatures of the catalyst bed. Typically, 0.3 g of catalyst pellets in 20/30 mesh size was charged into the reactor. When necessary, the catalyst amount and pellet size were varied from 0.2 to 0.4 g and from 20/30 to 50/70 mesh, respectively. A feed gas stream consisting of 1500 ppm CH_4, 5% O_2, 0 or 10% H_2O and He balance was then supplied. The total gas flow rate was 850 mL min^{-1}, corresponding to a gas hourly space velocity (GHSV) of 100,000 h^{-1}. The long-term (50 h) activity test was also performed under wet conditions at two different temperatures (673 and 723 K). Prior to each activity test, the catalyst was pretreated with air flow at 773 K for 2 h. The concentrations of CH_4 and CO_2 were monitored online by a Thermo Nicolet 6700 FT-IR spectrometer with a 2 m gas cell. CH_4 was completely oxidized to CO_2 under O_2-rich feed gas stream where the partial oxidation of CH_4 was negligible over the entire temperature range examined [22]. The reaction rate (r) and turnover frequency (TOF) for CH_4 oxidation were calculated by the following equations [23]:

$$r(s^{-1}) = [(C_{CH4} \cdot X_{CH4} \cdot v)/(ML/MW)] \quad (1)$$

$$TOF(s^{-1}) = [(C_{CH4} \cdot X_{CH4} \cdot v)/(ML/MW \cdot D)] \quad (2)$$

where C_{CH4} is the concentration of CH_4 (mol L^{-1}) in feed gas stream, X_{CH4} the conversion of CH_4 (%), v the volumetric flow rate (L s^{-1}), ML the Pd loading on the catalyst (g), MW the molecular weight of Pd (106.42 g mol^{-1}), and D the Pd dispersion (%) determined from CO chemisorption. Both the reaction rate and TOF value, where the CH_4 oxidation is primarily controlled by surface reaction, were obtained for CH_4 conversions less than 15%. The apparent activation energy (E_{app}) was calculated from the slope of the Arrhenius plot for this reaction.

2.3. Catalyst characterization

Powder X-ray diffraction (XRD) patterns were measured on a PANalytical X'Pert diffractometer (Cu Kα radiation) with an X'Celerator detector. Elemental analysis for Si, Al, and Pd was performed on a combination of Shimadzu ICPE-9000 inductively coupled plasma and Perkin-Elmer 5000 atomic absorption spectrophotometer. Pd particle size and location were determined by a JEOL JEM-2010 transmission electron microscope (TEM) operating at an accelerating voltage of 200 kV. N_2 sorption experiments were carried out on a Mirae SI Nanoporosity-XG analyzer. H_2O temperature-programmed desorption (TPD) measurements were performed on a fixed-bed, flow-type apparatus attached to a Hewlett-Packard 5890 series II gas chromatograph with a thermal conductivity detector. 0.1 g of catalyst powder were pretreated with He flow (30 mL min^{-1}) at 823 K for 2 h. Then, 7% H_2O vapor (30 mL min^{-1}) was passed over the sample at room temperature

Table 2
Physicochemical properties of supported Pd catalysts prepared in this work.

Catalyst ID[a]	Zeolite support structure	Si/Al[b]	Pd[b] (wt%)	BET surface area[c] ($m^2\ g^{-1}$)			Pd dispersion[d] (%)	
				support[e]	fresh	used[f]	fresh	used[f]
1.2Pd-SSZ-13(6)	CHA	6	1.2	710	610	–[g]	1.7	–[g]
0.5Pd-SSZ-13(16)		16	0.5	750	670	–[g]	3.5	–[g]
1.1Pd-SSZ-13(16)			1.1		660	650	6.8	5.7
2.2Pd-SSZ-13(16)			2.2		650	–[g]	3.5	–[g]
4.0Pd-SSZ-13(16)			4.0		650	–[g]	1.9	–[g]
1.2Pd-SSZ-13(27)		27	1.2	840	730	–[g]	4.0	–[g]
1.0Pd-LTA(16)	LTA	16	1.0	760	650	640	3.9	1.9
1.2Pd-PST-7(11)	UFI	11	1.2	690	570	550	3.0	2.0
1.0Pd-RTH(10)	RTH	10	1.0	610	560	550	5.0	3.2
1.3Pd-ZSM-5(14)	MFI	14	1.3	400	340	320	5.5	4.2
1.1Pd-Al_2O_3	–	–	1.1	200	190	170	23.3	22.0

[a] The first number is the Pd loading level in wt%, and the last number in parentheses is the bulk Si/Al ratio of the zeolite support.
[b] Determined by elemental analysis.
[c] Calculated from N_2 adsorption data.
[d] Determined by CO chemisorption.
[e] The proton form of zeolite supports or pure γ-Al_2O_3.
[f] The catalysts recovered after the reaction under wet feed conditions at 723 K for 50 h.
[g] Not determined.

for 0.5 h. The treated sample was subsequently purged with He (100 mL min^{-1}) at the same temperature for 1 h. The TPD profile was obtained in flowing He (30 mL min^{-1}) from room temperature to 823 K with a heating rate of 5 K min^{-1}. NH_3 TPD measurements were carried out on the same apparatus as that used for H_2O TPD, following the procedures described in our previous work [24]. Pulsed CO chemisorption was conducted on a Micromeritics AutoChem II 2920 analyzer to measure Pd dispersion. Details of the measurements are given elsewhere [25].

The ^{27}Al MAS NMR spectra were recorded on a Bruker Avance 500 spectrometer at a spinning rate of 10.0 kHz. The operating ^{27}Al frequency was 130.318 MHz, and the spectra were obtained with an acquisition of 1024 pulse transients, which were repeated with a pulse length of 2.0 μs and a recycle delay of 0.1 s The ^{27}Al chemical shifts are reported relative to an $Al(H_2O)_6^{3+}$ solution. The X-ray adsorption near edge spectra (XANES) at the Pd K-edge were collected on the 7D1 beam line at the Pohang Accelerator Laboratory (PAL), Pohang, Korea, using a Si (111) crystal monochromator and ionization chambers. Pd foil was employed for the energy calibration (E_0 = 24,350 eV). The physicochemical properties of supported Pd catalysts prepared here are listed in Table 2.

3. Results and discussion

3.1. Catalytic performance

Fig. 1 shows CH_4 conversion as a function of temperature in CH_4 combustion over Pd catalysts supported on four cage-based, small-pore zeolites with different framework structures, i.e., 1.1Pd-SSZ-13(16), 1.0Pd-LTA(16), 1.2Pd-PST-7(11), and 1.0Pd-RTH(10), as well as over 1.1Pd-Al_2O_3 and 1.3Pd-ZSM-5(14), measured at 100,000 h^{-1} GHSV and 1500 ppm CH_4, 5% O_2, and 0 or 10% H_2O in the feed. Table 3 lists their T_{50} values under both dry and wet conditions. These catalytic results will allow us to conjecture the effects of zeolite support structure and acidity on the CH_4 oxidation activities of supported Pd catalysts, because both the Pd contents (1.0–1.3 wt%) and support Si/Al ratios (10–16) are similar to one another (Table 2). When no water vapor exists in the feed, 1.1Pd-Al_2O_3 is characterized by the lowest T_{50} value (580 K) among the catalysts tested here. It was also found that the T_{50} value of zeolite-supported Pd catalysts is higher in the order 1.1Pd-SSZ-13(16) < 1.3Pd-ZSM-5(14) < 1.0Pd-RTH(10) < 1.0Pd-LTA(16) < 1.2Pd-PST-7(11). Considering that 1.1Pd-SSZ-13(16) is more active than 1.3Pd-ZSM-5(14) with an intersecting 10-ring pore system between the straight (5.6 × 5.3 Å) and the sinusoidal (5.5 × 5.1 Å) channels (Table 1), its 8-ring windows with pore dimensions of 3.8 × 3.8 Å may be large enough to allow the free diffusion of CH_4 with a kinetic diameter of 3.8 Å in the reaction temperature region employed in this work.

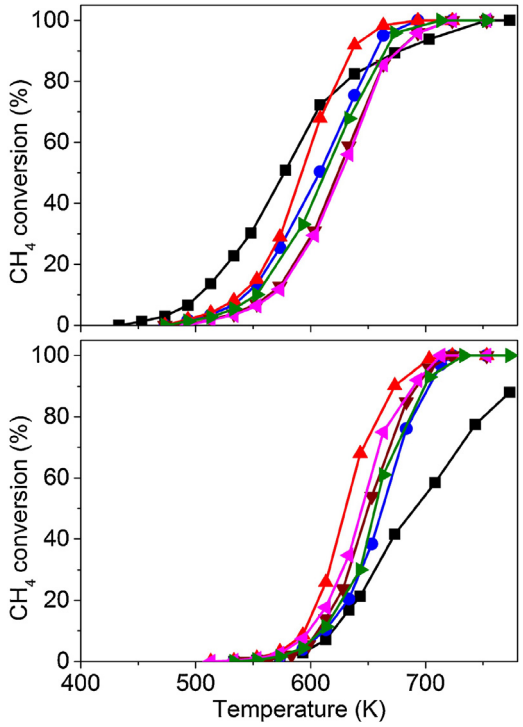

Fig. 1. CH_4 conversion as a function of temperature in CH_4 oxidation over 1.1Pd-Al_2O_3 (■), 1.3Pd-ZSM-5(14) (●), 1.1Pd-SSZ-13(16) (▲), 1.0Pd-LTA(16) (▼), 1.2Pd-PST-7(11) (◀), and 1.0Pd-RTH(10) (▶) under dry (top) and wet (bottom) feed conditions. The feed contains 1500 ppm CH_4, 5% O_2, and 0 or 10% H_2O balanced with He at 100,000 h^{-1} GHSV.

It is also remarkable that no noticeable changes in the CH_4 oxidation activity of 1.1Pd-SSZ-13(16) were caused by varying the feed gas flow rate from 570 to 1130 mL min^{-1} or by decreasing the catalyst pellet size from 20/30 to 50/70 mesh (Fig. S1). Thus, the mass transfer effects on the oxidation activity of Pd catalysts under the reaction conditions studied here appear to be negligible. As expected, on the other hand, all catalysts showed a signifi-

Table 3
Catalytic performance of a series of supported Pd catalysts with different metal contents and different supports for CH_4 combustion.

Catalyst ID[a]	T_{50}^{dry} [b] (K)	T_{50}^{wet} [b] (K)	ΔT_{50} [c] (K)	E_{app}^{dry} [d] (kJ mol^{-1})	E_{app}^{wet} [d] (kJ mol^{-1})	TOF^{dry} [e] $\times 10^2$ (s^{-1})	TOF^{wet} [f] $\times 10^2$ (s^{-1})
1.2Pd-SSZ-13(6)	630	700	70	77	141	1.7	1.4
0.5Pd-SSZ-13(16)	650	720	70	77	141	1.6	0.9
1.1Pd-SSZ-13(16)	590	630	40	77	141	1.7	3.6
2.2Pd-SSZ-13(16)	590	630	40	77	141	1.6	3.5
4.0Pd-SSZ-13(16)	590	630	40	77	141	1.7	3.5
1.2Pd-SSZ-13(27)	610	640	30	77	141	1.7	4.2
1.0Pd-LTA(16)	620	650	30	76	141	1.5	4.4
1.2Pd-PST-7(11)	630	640	10	77	141	1.5	6.3
1.0Pd-RTH(10)	610	650	40	77	142	1.6	2.6
1.3Pd-ZSM-5(14)	600	660	60	78	142	1.6	1.8
1.1Pd-Al_2O_3	580	690	110	76	139	1.6	0.3

[a] The same as the catalyst IDs in Table 2.
[b] Light-off temperature under dry or wet feed conditions.
[c] $\Delta T_{50} = T_{50}^{wet} - T_{50}^{dry}$.
[d] Calculated from the slope of the Arrhenius plot for CH_4 combustion.
[e] Determined at 513 K.
[f] Determined at 593 K.

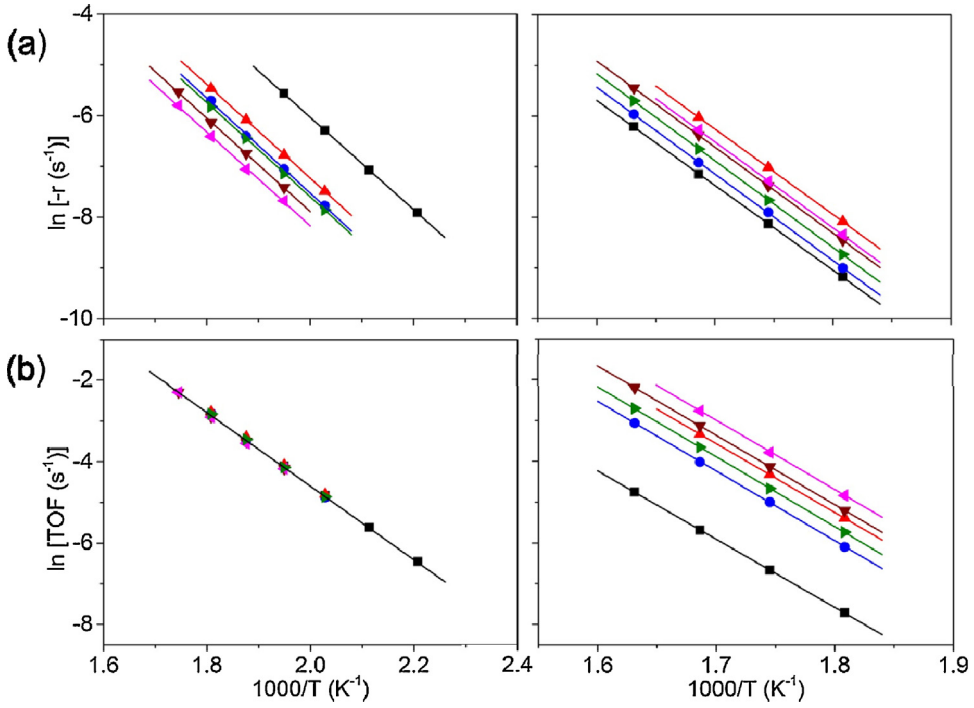

Fig. 2. (a) Reaction rates and (b) TOF values for CH_4 oxidation over 1.1Pd-Al_2O_3 (■), 1.3Pd-ZSM-5(14) (●), 1.1Pd-SSZ-13(16) (▲), 1.0Pd-LTA(16) (▼), 1.2Pd-PST-7(11) (◀), and 1.0Pd-RTH(10) (▶) under dry (left) and wet (right) feed conditions.

cant decrease in CH_4 oxidation activity when the feed contains 10% water vapor. The largest decrease in activity is observed for 1.1Pd-Al_2O_3, making it worse than any of five zeolite-supported Pd catalysts. It has been repeatedly shown that the PdO species in Al_2O_3 can be readily transformed into less active $Pd(OH)_2$ under wet conditions [3,5,6]. Of particular interest is that the extent of decrease by water vapor is significantly altered according to the structure type of zeolite supports: the T_{50} value is now in the order 1.1Pd-SSZ-13(16) < 1.2Pd-PST-7(11) < 1.0Pd-LTA(16) < 1.0Pd-RTH(10) < 1.3Pd-ZSM-5(14). Therefore, it is clear that the CH_4 oxidation activity of 1.1Pd-SSZ-13(16) is best under both dry and wet conditions among the five zeolite-supported Pd catalysts. Under wet conditions, in addition, the cage-based, small-pore zeolites are more efficient as a Pd support than the channel-based, medium-pore zeolite ZSM-5, the most widely studied zeolite support for this reaction [8–13].

Fig. 2 compares the reaction rates and TOF values for CH_4 oxidation over a series of supported Pd catalysts described above. Despite the similarity (1.0–1.3 wt%) in Pd content, their reaction rates are fairly different from one another under both dry and wet conditions, as revealed by the catalytic results in Fig. 1. Under dry conditions, however, no noticeable differences in the E_{app} value (76–78 kJ mol^{-1}), as well as in the TOF value (1.5–1.7 $\times 10^{-2}$ s^{-1} at 513 K), are observed. This indicates that the active sites in these six supported Pd catalysts have quite similar CH_4 oxidation activities to one another, whereas there are considerable differences in their Pd dispersion (Table 2). Considering the structure-insensitive nature of CH_4 oxidation, in fact, it is not surprising that the Pd catalyst with a higher dispersion shows a higher CH_4 oxidation activity [12,26]. The presence of 10% water vapor in the feed also led to no significant differences in the apparent activation energy (139–142 kJ mol^{-1}) of the above-described Pd catalysts. However, the fact that the E_{app} values are approximately 1.8 times higher under wet conditions than under dry conditions indicates that CH_4 oxidation over supported Pd catalysts is severely inhibited by water adsorption mainly on the catalyst support. The large difference in

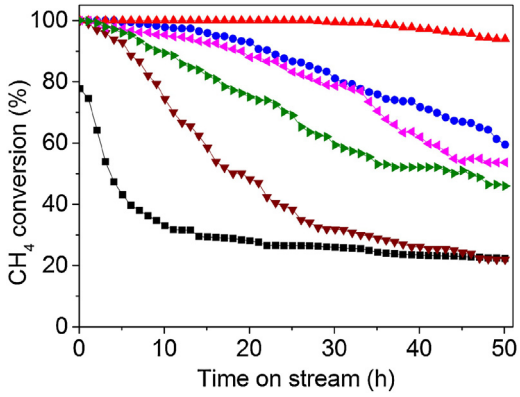

Fig. 3. Long-term performance of 1.1Pd-Al_2O_3 (■), 1.3Pd-ZSM-5(14) (●), 1.1Pd-SSZ-13(16) (▲), 1.0Pd-LTA(16) (▼), 1.2Pd-PST-7(11) (◀), and 1.0Pd-RTH(10) (▶) for CH_4 combustion under wet feed conditions at 723 K. The feed contains 1500 ppm CH_4, 5% O_2, and 10% H_2O balanced with He at 100,000 h^{-1} GHSV.

TOF between zeolite-supported Pd catalysts and 1.1Pd-Al_2O_3 can be explained by the less hydrophilic nature of high-silica zeolite supports, leading to the adsorption of a smaller amount of H_2O.

The catalytic results in Table 3 also show that large differences in the TOF value (1.8–6.3 × 10^{-2} s^{-1} at 593 K) are observed for the five Pd catalysts supported on different zeolites when the reaction is carried out under wet conditions. This indicates that the interactions of intrazeolitic Pd species with water differ considerably according to the structure type of zeolite support used. It is worth noting that among the zeolite-supported Pd catalysts studied here, 1.2Pd-PST-7(11) shows the smallest difference (10 K) between the light-off temperature (T_{50}^{wet}) obtained under wet conditions and that (T_{50}^{dry}) under dry conditions, although the precise reason remains unclear. The long-term performance of six catalysts with similar Pd contents but different supports for CH_4 oxidation under wet conditions at 723 K is compared in Fig. 3. It can be seen that the deactivation behavior of Pd catalysts also depends on the type of catalyst support employed. 1.1Pd-SSZ-13(16) shows a negligible decrease in CH_4 conversion over the period (50 h) of time on stream studied, rendering it considerably more stable even than 1.3Pd-ZSM-5(14). By contrast, the opposite holds for 1.0Pd-LTA(16). As shown in Fig. 3, its conversion at 50 h on stream becomes the same as that of 1.1Pd-Al_2O_3 under wet conditions. We also carried out the durability test at a lower reaction temperature (673 K) where their initial CH_4 conversions were ca. 90% or lower. No significant differences in the trend of catalyst deactivation were observed (Fig. S2).

3.2. Characteristics of supported Pd

Powder XRD measurements reveal that the structures of all the zeolite supports remain intact after the long-term activity test at 723 K in the presence of 10% H_2O vapor (Fig. S3). An X-ray peak around $2\theta = 33.8^\circ$, assignable to the (002) reflection of the tetragonal PdO phase, is detectable from the fresh and used forms of five zeolite-supported Pd catalysts. However, none of them gave a peak around $2\theta = 40.2^\circ$, corresponding to the (111) reflection of metallic Pd (Pd^0) phase. The lack of Pd^0 in all Pd catalysts in this work can be further confirmed by Pd K-edge XANES analysis (Supplementary Fig. S4): the spectra of Pd catalysts are always the same as the spectrum of PdO, even after 50 h of the reaction at 723 K under wet conditions, regardless of the structure type of catalyst support employed. It is also remarkable that a non-negligible decrease in N_2 BET surface area is observed for each zeolite support when exchanged with Pd^{2+} ions and then calcined in air at 773 K (Table 2), mainly due to the formation of intrazeolitic PdO. However, there are no notable differences in the BET surface area between the fresh and used forms of each Pd catalyst. This indicates that all the zeolite supports are robust enough to maintain their structural integrity even after the long-term test under wet conditions at 723 K, which is in line with the powder XRD results in Supplementary Fig. S3.

Fig. 4 shows the TEM images of 1.3Pd-ZSM-5(14), 1.1Pd-SSZ-13(16), and 1.0Pd-LTA(16) before and after the long-term CH_4 combustion at 723 K in the presence of 10% water vapor. It is well established that during TEM measurements, the zeolite framework structure can be easily damaged by the incident electron beam, resulting in sintering of very small, intrazeolitic metal particles (<1 nm) [24,27]. Despite this, it is clear that the size and dispersion degree of particles in both fresh and used catalysts are larger and lower in the order 1.1Pd-SSZ-13(16) < 1.3Pd-ZSM-5(14) < 1.0Pd-LTA(16), respectively, which is directly opposite to their CH_4 conversion order after 50 h of the reaction under wet conditions at 723 K (Fig. 3). Small (~2 nm), well-dispersed PdO particles can be observed throughout the fresh 1.1Pd-SSZ-13(16) crystal, implying that they are mainly located within the SSZ-13 pores. Since somewhat larger (~5 nm) particles are easily detectable on the fresh 1.3Pd-ZSM-5(14) crystal edges, in addition, it appears that most of intrazeolitic PdO species were migrated and then agglomerated during calcination in air at 773 K for 5 h, suggesting their weaker interactions with the ZSM-5 framework than with the SSZ-13 framework. This is more evident for 1.0Pd-LTA(16) with the poorest long-term performance (Fig. 3) where considerably bigger particles are observed for its both fresh and used forms.

Further evidence to support the speculation given above can be obtained from the Pd dispersion data in Table 2 determined by CO chemisorption. 1.1Pd-Al_2O_3 has a much higher Pd dispersion than the zeolite-supported catalysts with similar Pd contents, which is even true for its used form, in good agreement with the TEM results in Fig. S5, due to the stronger metal-support interactions within the former catalyst [10]. The easy formation of $Pd(OH)_2$ in this catalyst under wet conditions is well established to be the main cause of a significant decrease in CH_4 conversion similar to that found in Fig. 3 [3,5,6]. It should also be noted that not only the Pd dispersion (6.8%) of fresh 1.1Pd-SSZ-13(16), but also the extent (16%) of its decrease after 50 h of CH_4 combustion at 723 K in the presence of 10% water vapor are highest and smallest among the zeolite-supported Pd catalysts, respectively. Therefore, it is most likely that the Pd catalyst is more stable when supported on SSZ-13 rather than on the other four zeolites with different framework topologies.

3.3. Role of zeolites as a Pd support

To check whether differences in the extent of catalyst activity decrease by water vapor originate mainly from those in the support structure itself or in its water adsorption behavior, we performed H_2O TPD measurements on five zeolite-supported catalysts with similar Pd contents (1.0–1.3 wt%), as well as on 1.1Pd-Al_2O_3. Besides two H_2O desorption peaks with temperature maxima around 380 and 430 K, the TPD profile of 1.1Pd-Al_2O_3 shows a broad desorption peak located around 550 K, which is similar to the profile shape reported for γ-Al_2O_3 [28]. As can be found in Fig. S6 and Table S1, in addition, the TPD profiles for zeolite-supported Pd catalysts are always characterized by two desorption peaks with maxima in the temperature regions 370–390 and 420–440 K. It thus appears that unlike the case of 1.1Pd-Al_2O_3 with stronger water-support interactions, the activity differences among the five zeolite-supported Pd catalysts in the presence of water vapor are mainly due to differences in the zeolite support structure.

Fig. 5 shows the ^{27}Al MAS NMR spectra of 1.3Pd-ZSM-5(14), 1.1Pd-SSZ-13(16), and 1.0Pd-LTA(16) before and after CH_4 combustion under wet conditions at 723 K for 50 h on stream. Here, the height of a more intense ^{27}Al resonance at 55–60 ppm, typical

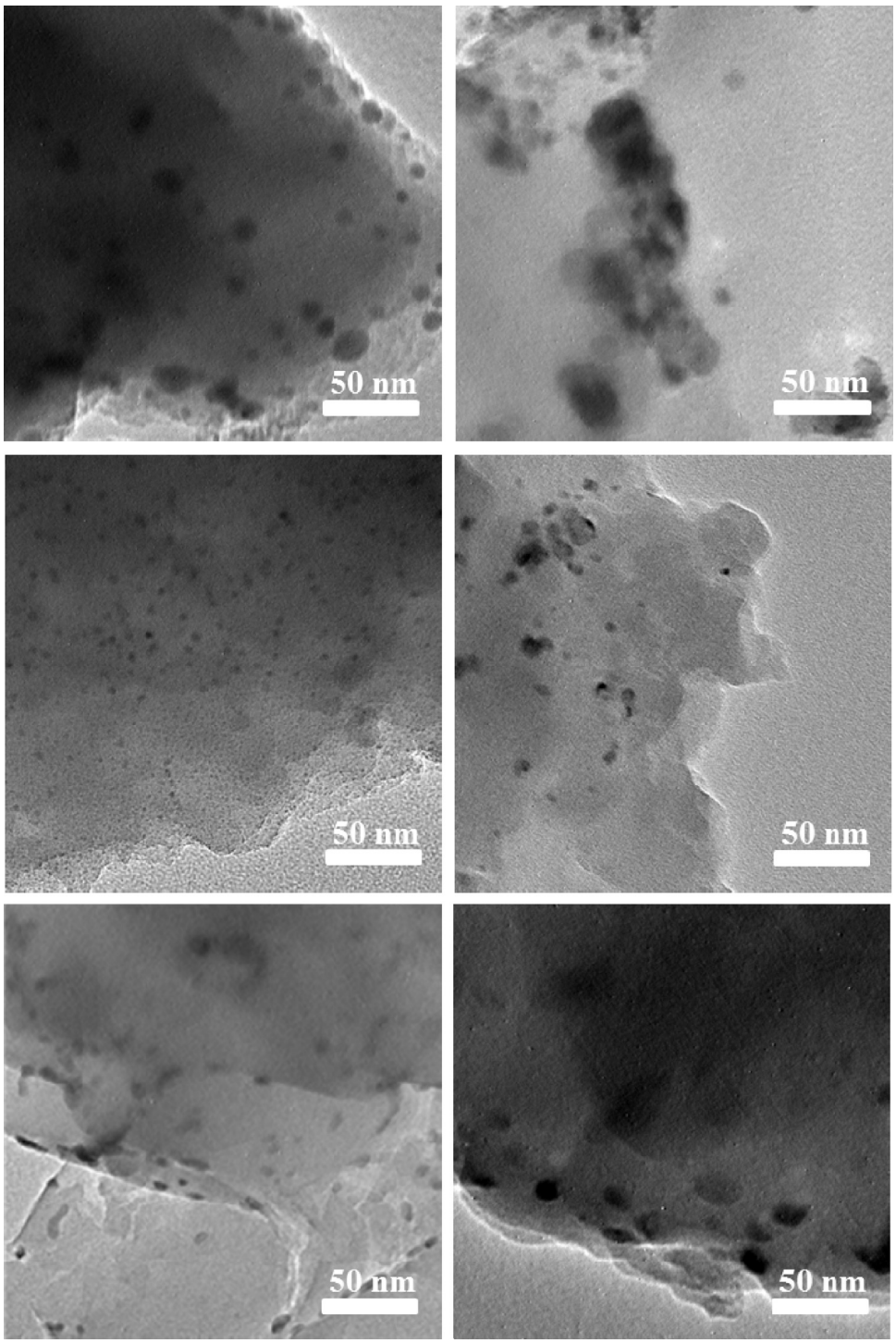

Fig. 4. TEM images of (from bottom to top) 1.3Pd-ZSM-5(14), 1.1Pd-SSZ-13(16), and 1.0Pd-LTA(16) before (left) and after (right) CH_4 oxidation under wet feed conditions at 723 K for 50 h on stream.

of tetrahedral Al in the zeolite framework, in each spectrum was adjusted on a similar scale in order to more clearly uncover the intensity difference with the resonance due to extraframework Al species around 0 ppm, as well as the spectral changes caused by durability test. All the ^{27}Al MAS NMR spectra in Fig. 5 show both tetrahedral and octahedral resonances. However, we note that the relative intensity of the octahedral resonance to the tetrahedral one from both fresh and used forms of these three Pd catalysts is higher in the order 1.1Pd-SSZ-13(16) < 1.3Pd-ZSM-5(14) < 1.0Pd-LTA(16), which is the same as the size order of their PdO particles (Fig. 4). Unlike the case of 1.3Pd-ZSM-5(14) and 1.0Pd-LTA(16), furthermore, 1.1Pd-SSZ-13(16) gave no noticeable increase in relative intensity of the octahedral resonance even after 50 h of the reaction under wet conditions at 723 K, revealing no evidence of significant delaumination during the long-term test.

Very recently, we have reported that divalent copper ions when fully exchanged into high-silica (Si/Al = 16–23) LTA zeolites exhibit excellent activity maintenance for NH_3-SCR even after aging at 1173 K in the presence of 10% water vapor, where the structure of the current commercial Cu-SSZ-13 catalyst for this reaction is

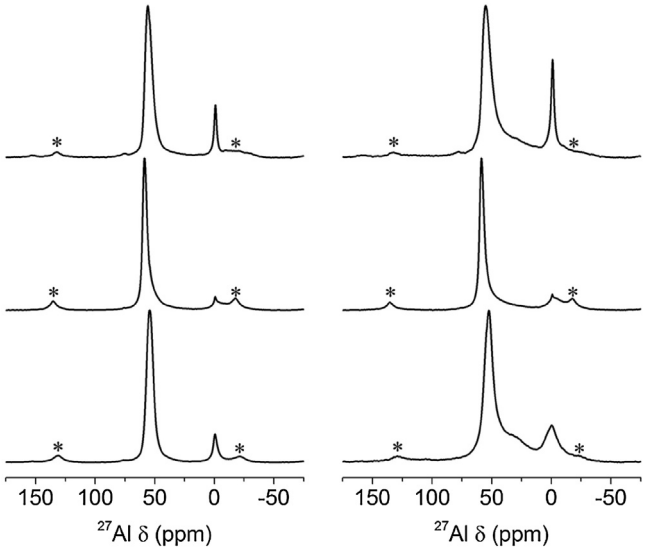

Fig. 5. ^{27}Al MAS NMR spectra of (from bottom to top) 1.3Pd-ZSM-5(14), 1.1Pd-SSZ-13(16), and 1.0Pd-LTA(16) before (left) and after (right) CH_4 combustion under wet feed conditions at 723 K for 50 h on stream. Spinning side bands are marked by asterisks.

completely collapsed [19]. However, we found no clear signs of delaumination in aged Cu-LTA catalysts with Cu contents of ca. 3 wt% or lower, although the aging temperature applied is higher by 450 K than the reaction temperature (723 K) of the long-term test of this work. The zeolite framework can function as a "huge ligand" to coordinate and stabilize its metal cations. If such is the case, then the nature and extent of metal-zeolite interactions should depend primarily not only on the type of metal cations introduced, but also on the structure type of zeolite supports. Notable differences in the stability of Pd-LTA and Cu-LTA (and also of Pd-SSZ-13 and Cu-SSZ-13) strongly support this argument, because the intrazeolitic location of metal species, as well as their state, in a particular zeolite structure can differ significantly according to their type.

Fig. 6 shows the NH_3 TPD profiles of the proton form of five zeolite supports with different topologies but similar Si/Al ratios (i.e., H-ZSM-5(14), H-SSZ-13(16), H-LTA(16), H-PST-7(11), and H-RTH(10)). All these TPD profiles are characterized by two desorption peaks corresponding to NH_3 desorption from weak and strong acid sites, respectively. However, their acid strength distributions are fairly different from one another. We also found that the high-temperature desorption peak from H-SSZ-13(16) is located at a higher temperature (maximum around 770 K) than that from any of the other four zeolite supports, indicative of a higher strength of its strong acid sites. This trend remains not only after Pd^{2+} ion exchange but only after durability test under wet conditions at 723 K, although a new NH_3 desorption peak with maximum around 680 K, attributable to the formation of intrazeolitic PdO species, is resolved in the NH_3 TPD profiles from all fresh zeolite-supported Pd catalysts, especially from fresh 1.3Pd-ZSM-5(14).

Fig. 6 also shows the appearance of another new desorption peak around 580 K, assignable to agglomerated PdO species [13], after the long-term reaction at 723 K, which can be correlated with an intensity decrease of the desorption peak around 680 K. It should be noted here that the extent of decrease in intensity of the high-temperature desorption peak appearing around 700 K or higher is fairly smaller for used 1.1Pd-SSZ-13(16) than for the other four used zeolite-supported catalysts. As a result, the density of strong acid sites is higher for the former catalyst, again showing its higher resistance to dealumination. This can also explain why 1.1Pd-SSZ-13(16) with the best long-term performance under wet conditions has a higher Pd dispersion than the other zeolite-supported catalysts with similar Pd contents (Table 2). Given that the strength of acid sites in zeolites can depend on the local structures around them [29,30], the framework topology of zeolite support employed appears to be the most important factor governing the CH_4 oxidation activity of the supported Pd catalyst.

3.4. Optimized catalyst composition

The results presented so far indicate that SSZ-13 is best among the Pd supports employed here. To optimize the Pd content and zeolite acidity in Pd-SSZ-13 catalyst, we prepared three SSZ-13 zeolites with Si/Al ratios of 6, 16, and 27, loaded different amounts (0.5–4.0 wt%) of Pd on them, and tested the CH_4 oxidation activities of the resulting catalysts. As shown in Table 3 and Fig. S7, no differences in the T_{50} value under both dry and wet conditions are observed when the Pd loading level on SSZ-13 with Si/Al = 16 is higher than 1.0 wt%. Powder XRD experiments reveal that the formation of agglomerated PdO is more noticeable at higher Pd contents (Fig. S8) and is accompanied by a decrease in Pd dispersion (Table 2). While this can be further supported by the NH_3 TPD results in Fig. S9, both increase and decrease in Si/Al ratio gave no better Pd dispersion (Table 2) and were not beneficial to CH_4

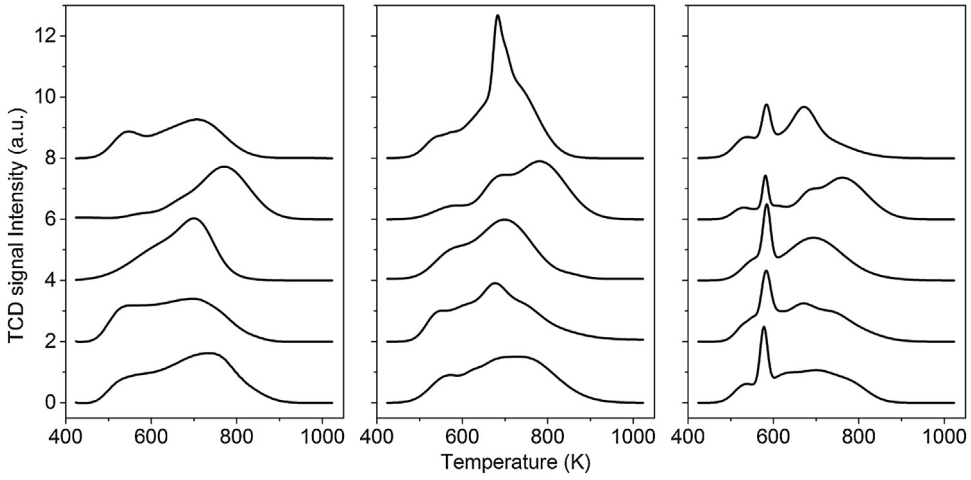

Fig. 6. NH_3 TPD profiles of (left, from top to bottom) H-ZSM-5(14), H-SSZ-13(16), H-LTA(16), H-PST-7(11), and H-RTH(10) and of the fresh (middle) and used (right) forms of (from top to bottom) 1.3Pd-ZSM-5(14), 1.1Pd-SSZ-13(16), 1.0Pd-LTA(16), 1.2Pd-PST-7(11), and 1.0Pd-RTH(10). Used zeolite-supported Pd catalysts were obtained by reacting the corresponding fresh catalysts with 1500 ppm CH_4, 5% O_2, and 10% H_2O balanced with He at 723 K and 100,000 h^{-1} GHSV for 50 h on stream.

combustion (Fig. S7). Thus, there appears to be the optimum Pd content (~1.0 wt%) and support Si/Al ratio (~15) leading to the best oxidation activity of Pd-SSZ-13.

4. Conclusions

The CH_4 combustion activities of Pd catalysts loaded on SSZ-13, LTA, PST-7, and RTH with similar bulk Si/Al ratios (10–16) have been compared with those of Pd-ZSM-5 and Pd-Al_2O_3 with similar Pd contents (ca. 1.0 wt%). When the feed contains 10% water vapor, the Pd catalysts supported on all these cage-based, small-pore zeolites are more active than Pd-ZSM-5 with two intersecting 10-ring channels, the most widely studied support for this reaction. In particular, Pd-SSZ-13, the light-off temperature of which is lower than that of any of the other zeolite-supported Pd catalysts, also showed the best durability under wet feed conditions. The strong acidity of SSZ-13 compared to the other four zeolites with different framework topologies appears to be the key to providing the Pd catalyst supported on SSZ-13 with stronger interactions between the intrazeolitic PdO species and the zeolite framework and thus to suppressing both the PdO sintering and dealumination in a more efficient manner during CH_4 combustion. The Pd content and support Si/Al ratio which can maximize the oxidation activity of Pd-SSZ-13 were found to be ca. 1.0 wt% and 16, respectively.

Acknowledgements

This work was supported by the National Creative Research Initiative Program (2012R1A3A2048833) through the National Research Foundation of Korea. We thank PAL for XANES beam time. PAL is supported by MSIP and POSTECH.

Appendix A. Supplementary data

Supplementary data associated with this article can be found, in the online version, at http://dx.doi.org/10.1016/j.apcatb.2017.07.032.

References

[1] Z. Li, G.B. Hoflund, J. Nat. Gas Chem. 12 (2003) 153–160.
[2] M. Cargnello, J.J. Delgado Jaén, J.C. Hernández Garrido, K. Bakhmutsky, T. Montini, J.J. Calvino Gámez, R.J. Gorte, P. Fornasiero, Science 337 (2012) 713–717.
[3] R. Gholami, M. Alyani, K.J. Smith, Catalysts 5 (2015) 561–594.
[4] P. Gélin, M. Primet, Appl. Catal. B 39 (2002) 1–37.
[5] D. Roth, P. Gélin, M. Primet, E. Tena, Appl. Catal. A 203 (2000) 37–45.
[6] J.-H. Park, J.-H. Ahn, H.-I. Sim, G. Seo, H.S. Han, C.-H. Shin, Catal. Commun. 56 (2014) 157–163.
[7] P. Araya, S. Guerrero, J. Robertson, F.J. Gracia, Appl. Catal. A 283 (2005) 225–233.
[8] C.-K. Shi, L.-F. Yang, X.-E. He, J.-X. Cai, Chem. Commun. (2002) 2006–2007.
[9] K. Okumura, E. Shinohara, M. Niwa, Catal. Today 117 (2006) 577–583.
[10] Y. Li, J.N. Armor, Appl. Catal. B 3 (1994) 275–282.
[11] C.-J. Liu, K. Yu, Y.-P. Zhang, X. Zhu, F. He, B. Eliasson, Appl. Catal. B 47 (2004) 95–100.
[12] J.-H. Park, B. Kim, C.-H. Shin, G. Seo, S.H. Kim, S.B. Hong, Top. Catal. 52 (2009) 27–34.
[13] Y. Lou, J. Ma, W. Hu, Q. Dai, L. Wang, W. Zhan, Y. Guo, X.-M. Cao, Y. Guo, P. Hu, G. Lu, ACS Catal. 6 (2016) 8127–8139.
[14] C. Baerlocher L.B. McCusker, Database of Zeolite Structures, http://www.iza-structure.org/databases/ (Accessed May 01, 2017).
[15] P. Tian, Y. Wei, M. Ye, Z. Liu, ACS Catal. 5 (2015) 1922–1938.
[16] I. Bull, R. S. Boorse, W. M. Jaglowski, G. S. Koermer, A., Moini, J. A. Patchett, W. M. Xue, P. Burk, J. C. Dettling, M. T. Caudle, U.S. Patent 0,226,545, 2008.
[17] D. Jo, T. Ryu, G.T. Park, P.S. Kim, C.H. Kim, I.-S. Nam, S.B. Hong, ACS Catal. 6 (2016) 2443–2447.
[18] D. Jo, J.B. Lim, T. Ryu, I.-S. Nam, M.A. Camblor, S.B. Hong, J. Mater. Chem. A 3 (2015) 19322–19329.
[19] T. Ryu, N.H. Ahn, S. Seo, J. Cho, H. Kim, D. Jo, G.T. Park, P.S. Kim, C.H. Kim, E.L. Bruce, P.A. Wright, I.-S. Nam, S.B. Hong, Angew. Chem. Int. Ed. 56 (2017) 3256–3260.
[20] S.I. Zones, R.A. Van Nordstrand, Zeolites 8 (1988) 166–174.
[21] P.S. Kim, M.K. Kim, B.K. Cho, I.-S. Nam, S.H. Oh, J. Catal. 301 (2013) 65–76.
[22] X. Weng, H. Ren, M. Chen, H. Wan, ACS. Catal. 4 (2014) 2598–2604.
[23] Y.J. Kim, J.K. Lee, K.M. Min, S.B. Hong, I.-S. Nam, B.K. Cho, J. Catal. 311 (2014) 447–457.
[24] H.J. Jung, S.S. Park, C.-H. Shin, Y.-K. Park, S.B. Hong, J. Catal. 245 (2007) 65–74.
[25] S.B. Kang, H.J. Kwon, I.-S. Nam, Y.I. Song, S.H. Oh, Ind. Eng. Chem. Res. 50 (2011) 5499–5509.
[26] G. Zhu, J. Han, D.Y. Zemlyanov, F.H. Ribeiro, J. Am. Chem. Soc. 126 (2004) 9896–9897.
[27] M. Pan, Micron 27 (1996) 219–238.
[28] Y.T. Kim, K.-D. Jung, E.D. Park, Appl. Catal. A 393 (2011) 275–287.
[29] N. Katada, K. Suzuki, T. Noda, G. Sastre, M. Niwa, J. Phys. Chem. C 113 (2009) 19208–19217.
[30] K. Suzuki, G. Sastre, N. Katada, M. Niwa, Chem. Lett. 38 (2009) 354–355.